Bend-Twist Coupling Analysis of Composite Hydrofoils with FSI

V. TEMTCHING[a,b], B. AUGIER[c], J.-A. Astolfi[a]

Institut de Recherche de l'Ecole Navale,Brest-France. vanilla@seair.fr
SEAIR, 10 Rue chalutier les 2 anges, Lorient-France
IFREMER Brest-France. benoit.augier@ifremer.fr
jacques-andre.astolfi@ecole-navale.fr

Résumé

La conception d'hydrofoils de haute performances passe par un couplage entre simulations fluide avec prise en compte de surface libre et une analyse mécanique de ces appendices en composites sous chargements hydrodynamique. Selon le drapage utilisé dans ces composites, le chargement hydrodynamique peut faire intervenir le couplage flexion-torsion qui impacte les performances de l'hydrofoil, ce couplage est un effet cible pour les structures fortement chargées afin d'alléger leur chargement en réduisant l'angle d'incidence du foil.
Cette étude s'intéresse expérimentalement et numériquement à l'apparition du couplage flexion-torsion et de son influence sur les performances hydrodynamiques d'un hydrofoil traversant la surface libre. Quatre hydrofoils de section constante, géométriquement identiques avec des drapages composite différents sont étudiés. Les structures sont conçues pour avoir un déplacement en bout de foil de l'ordre de 5 à 10% d'envergure.
Les premières expériences sont réalisées en air afin de caractériser mécaniquement les structures et de visualiser la réponse en flexion des différents drapages. Les résultats mettent en évidence le couplage flexion-torsion qui se traduit par un angle de torsion sur les sections de l'hydrofoil. Une comparaison de ces résultats à une approche structurelle reposant sur la théorie des poutres par éléments finis, intégrant une modification des matrices de rigidité pour prendre en compte le couplage flexion-torsion, est réalisée et donne de bon résultats.
Des expériences hydrodynamiques sont également réalisées sur les hydrofoils et les résultats obtenus montrent une modification de leurs performances hydrodynamiques, dû au couplage flexion torsion.
Le code structurel est couplé à un code fluide de ligne portante pour l'analyse des interactions des structures fluides, et la comparaison avec les expériences hydrodynamiques donne d'excellents résultats (moins de 10 % d'écarts relatifs sur la prédiction des déplacements et la répartition des efforts).
Cette approche est une partie essentielle qui s'intègre dans le processus de pré-conception d'un hydrofoil et calcule l'effet d'une déformation passive sur les performances hydrodynamiques de ces structures et donc, de la stabilité globale du bateau.

Abstract

For the top high performances foiling yacht design, the design process is a complex combination of free surface hydrodynamic simulations, coupled with highly loaded composite's structural analysis.

Bend-twist coupling is a phenomenon that appears in composite materials, depending on its layup composition. It impacts the hydrofoil performances and therefore the fluid structure interactions applying on the hydrofoil. That coupling is a target effect for highly loaded structures to reduce the loads by reducing the flow 's angle of attack at the tip.
This study investigates experimentally and numerically the appearance of bend-twist coupling and its influence on the hydrodynamic performances of a surface piercing hydrofoil. Four hydrofoils with a constant chord, geometrically identical with different composite layups are investigated, the foils are designed to have a significant tip displacement of 5 to 10% of the span length.
The experiments are firstly performed in air to characterize the foils and investigate the BTC. The results highlight a bending-twist effect that lead to a twist angle on the hydrofoil sections. A comparison of that results to a structural approach from beam theory by finite elements, with modifications of the stiffness matrices to consider bend-twist coupling effect is preformed and give good agreement.
Hydrodynamic experiments on a flume are also performed on the hydrofoils and the results show significant changes in the hydrodynamic performances of the hydrofoils, due to the bend twist coupling effect. The structural code is coupled with a potential fluid code for fluid structure interactions analysis and the comparison to the hydrodynamic experiments give great results (less than 10% of relative discrepancies on the displacements prediction and loads distribution.
This approach is a strong brick to be used during the pre-design process, to compute the effect of passive deformation on hydrodynamic performances of the foils and therefore the yacht stability.

Key words: Bending-twist coupling, Composite materials, Fluid Structure Interactions, Hydrofoils.

Notation

BTC	Bend twist coupling
"FE"	Beam theory by Finite element
"FE-BTC"	"FE" with BTC implemented
E_l	UD 's Young modulus in longitudinal direction $[MPa]$
E_t	UD Young modulus in transverse direction direction $[MPa]$
FSI	Fluid structure Interactions
G_{lt}	Shear modulus of the UD $[MPa]$
G_m	Shear modulus of the resin $[MPa]$
ν_f	Poisson coefficient of the fiber
θ	Twist angle

1 Introduction

Composite structures are extensively used for the appendages in the sailing yacht domain, putting more complexity in their behavior prediction. Bend-twist coupling is a phenomenon that appears in these materials, depending on the orientation of the fibers in the layup. [2], shows a non zero percentage of bend twist coupling for carbon and glass fibers with any orientation of the plies in a range of $]0° - 90°[$ excepts from $0°$ and $90°$. The hydrodynamic forces added to the BTC effect which modifies the flow's angle of attack, lead to significant deformations of the hydrofoils which impact their hydrodynamic performances and therefore the global yacht equilibrium [1].
These structural deformations can have a devastating effect on the structures and are highlighted by the fluttering effect which appears on the keels. The bend-twist coupling in the lifting structures can be a good approach to control the lifting force through FSI with a passive adaptive method, the target is to reduce the loads by reducing the incidence at the tip. [3], [5] investigated the effect of this coupling on natural frequencies and mode shape to improve the design and the control of composite structures.

The present study investigates experimentally and numerically the appearance of BTC phenomenon on four hydrofoils geometrically identical with different composite layups. The foils are straight structures of $1.35m$ span and $0.114m$ constant chord. The section is a NACA 0015 sandwich structure made of an AIREX web and laminated skin illustrated in Fig 1. In the CAD image, the green AIREX is clearly visible, the orange part is the glue Spabond 345 and the white part is the glass fiber. The hydrofoil geometry is also show in the figure.

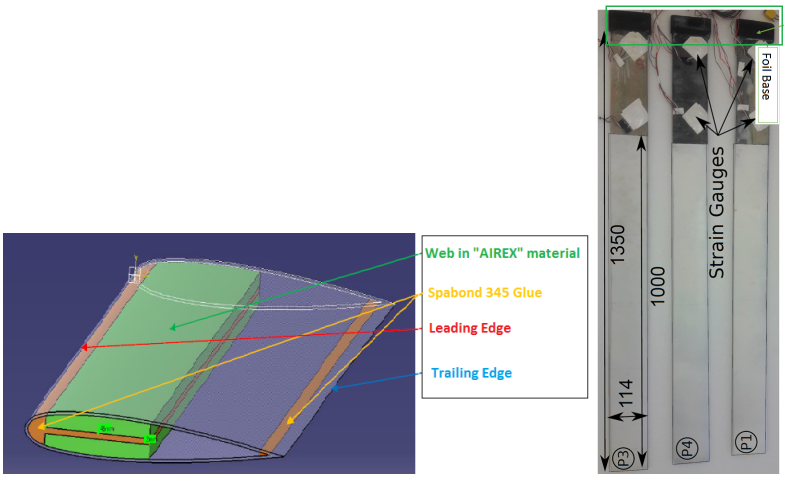

Figure 1: Hydrofoil geometry and description of the sandwich.

The four different layups and associated materials are given in Table 1.

Foils	Material	layup
P_1	Epoxy-Glass2	$[\pm 45)_2/0_{0.5}]_{sym}$
P_2	Epoxy-Glass1	$[(90/-45/0_{0.5}]_{sym}$
P_3	Epoxy-Glass1	$[(90/45/0_{0.5}]_{sym}$
P_4	Epoxy-Carbon	$[(90/0)_{sym}]$

Material	Carbon	Glass1	Glass2
$E_l[GPa]$	120	54	45
$E_t[GPa]$	10	10.4	10
$G_{lt}[GPa]$	4	3.9	5
ν_{lt}	0.362	0.25	0.25

Table 1: Hydrofoils Layups and Mechanical properties of the plies. The layup P_1 uses the Glass2 when layupP_2 and P_3 uses the Glass1.

The first chapter of this paper focuses on the theoretical background describing the structural method

used to approach the bend twist coupling effect on these structures under bending loads.
The second chapter is dedicated to the mechanical experiments performed in air on the four composite hydrofoils to characterize the foils and to investigate the BTC. The measurements are recorded with a laser and are to the results from the structural method approaching the BTC.
The last chapter presents the hydrodynamic experiments carried out in a flume with the hydrofoils piercing the free surface. The foils displacements and hydrodynamic forces are measured and compared to the results from the global brick analyzing FSI.
The principal objective of this paper is to measure the BTC effect on the hydrofoils and to validate the method implemented to approach this phenomenon.

2 Theoretical Background

In a first approach, the hydrofoil are consider as beam elements exhibiting displacements in the elastic domain. The structural analysis of the hydrofoils, stands on Euler-Bernoulli Beam equations, solved by finite elements. In the paper, "FE" will designates the present approach.
Figure 2 shows for example, a 1-element beam with the DOF on the two nodes. We have 3 DOF in translation and 3 DOF in rotation for each node which are the solution of the system (1).

$$K \times U = F \tag{1}$$

K: the stiffness Matrix in the global reference, the matrix is symmetric.
F: Forces applied to the structure in the global reference.
U: DOF of the structure.

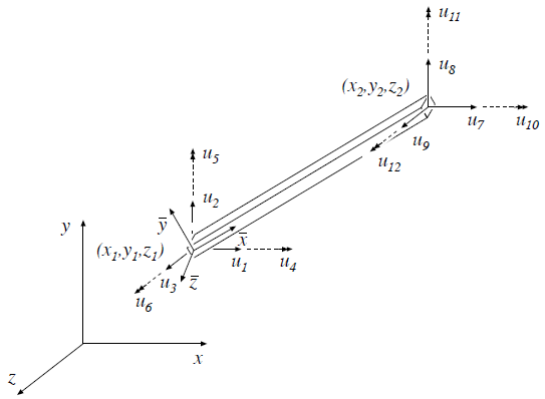

Figure 2: DOF of a 1 element beam. [4]

Figure 3 shows in details (Eq.1). BTC effect we are looking here is a twist angle u_4 or u_{10} induced by the bending forces $F_{2,3,5,6,8,9,11,12}$. The coupling terms linking them are usually neglected for quasi isotropic or orthotropic material in this theory and set to zero in the global stiffness matrix .

To consider bend twist coupling, [2] describes $\alpha[\%]$, the bend twist coupling percentage induced by a ply orientation in the composite layup. $\alpha[\%]$ defined by Eq. 2 depends on a coupling modulus g, the bending stiffness E and the torsional modulus GJ.

$$\begin{bmatrix} k_{11} & k_{12} & k_{13} & 0 & k_{15} & k_{16} & k_{17} & k_{18} & k_{19} & 0 & k_{111} & k_{112} \\ & k_{22} & k_{23} & 0 & k_{25} & k_{26} & k_{27} & k_{28} & k_{29} & 0 & k_{211} & k_{212} \\ & & k_{33} & 0 & k_{35} & k_{36} & k_{37} & k_{38} & k_{39} & 0 & k_{311} & k_{312} \\ & & & k_{44} & 0 & 0 & 0 & 0 & 0 & -k_{44} & 0 & 0 \\ & & & & k_{55} & k_{56} & k_{57} & k_{58} & k_{59} & 0 & k_{511} & k_{512} \\ & & & & & k_{66} & k_{67} & k_{68} & k_{69} & 0 & k_{611} & k_{612} \\ & & & & & & k_{77} & k_{78} & k_{79} & 0 & k_{711} & k_{712} \\ & & & & & & & k_{88} & k_{89} & 0 & k_{811} & k_{812} \\ & & & & & & & & k_{99} & 0 & k_{911} & k_{912} \\ & & & & \text{Sym} & & & & & k_{1010} & 0 & 0 \\ & & & & & & & & & & k_{1111} & k_{1112} \\ & & & & & & & & & & & k_{1212} \end{bmatrix} * \begin{pmatrix} u_1 \\ u_2 \\ u_3 \\ u_4 \\ u_5 \\ u_6 \\ u_7 \\ u_8 \\ u_9 \\ u_{10} \\ u_{11} \\ u_{12} \end{pmatrix} = \begin{pmatrix} F_1 \\ F_2 \\ F_3 \\ F_4 \\ F_5 \\ F_6 \\ F_7 \\ F_8 \\ F_9 \\ F_{10} \\ F_{11} \\ F_{12} \end{pmatrix}$$

Figure 3: Global stiffness matrix of the structure without BTC terms.

$$\alpha = \frac{g}{\sqrt{EI \times GJ}} \tag{2}$$

In the stiffness matrix, g links the bending motion b to the torsional moment M_t and the twist motion t to the bending moment M_b as shown in Eq.3.

$$\begin{bmatrix} EI & -g \\ -g & GJ \end{bmatrix} \begin{bmatrix} b \\ t \end{bmatrix} = \begin{bmatrix} M_b \\ M_t \end{bmatrix} \tag{3}$$

$\alpha[\%]$ is presented in the Fig 4 for the glass and carbon fibers and depicts that: for the same fiber orientations, the BTC is higher with carbon fiber than in glass fiber. All the plies orientation excepts from 0 ° and 90 ° lead to BTC phenomenon and the maximum coupling is obtained with plies orientation of around $\pm 25°$.

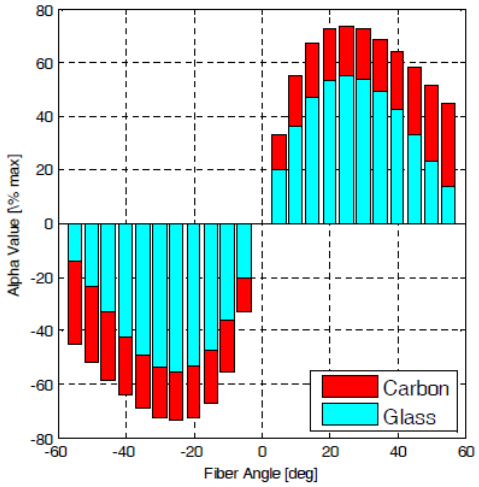

Figure 4: Limit of bend twist coupling percentage with the plies orientation for glass and carbon fibers. [2]

Thus the method implemented to approach the BTC, stands on the modification of the global stiffness matrix K (figure 3). The coupling coefficients previously set to zero are replaced by new terms c_{ij}, linking u_4, u_{10} to $F_{2,3,5,6,8,9,11,12}$.
These coupling terms c_{ij} expressed in Eq.4 depend on the coupling percentage $\alpha[\%]$, the bending stiffness k_{ii}, the torsional stiffness k_{ii} and proportion of plies in the laminate responsible of this coupling.

$$C_{ij} = \sum_{\beta=0}^{90} \alpha_\beta \times A_\beta \times \sqrt{k_{ii} \times k_{jj}} \tag{4}$$

β: is the ply orientation [°].
α_β: The maximum percentage of bend twist coupling induced by a ply, oriented at θ degrees.
A_β: the percentage of the ply oriented at θ degrees in the layup of the structure.

$$K = \begin{bmatrix} k_{11} & k_{12} & k_{13} & 0 & k_{15} & k_{16} & k_{17} & k_{18} & k_{19} & 0 & k_{111} & k_{112} \\ & k_{22} & k_{23} & c_{24} & k_{25} & k_{26} & k_{27} & k_{28} & k_{29} & c_{210} & k_{211} & k_{212} \\ & & k_{33} & c_{34} & k_{35} & k_{36} & k_{37} & k_{38} & k_{39} & c_{310} & k_{311} & k_{312} \\ & & & k_{44} & c_{45} & c_{46} & 0 & c_{48} & c_{49} & -k_{44} & c_{411} & c_{412} \\ & & & & k_{55} & k_{56} & k_{57} & k_{58} & k_{59} & c_{510} & k_{511} & k_{512} \\ & & & & & k_{66} & k_{67} & k_{68} & k_{69} & c_{610} & k_{611} & k_{612} \\ & & & & & & k_{77} & k_{78} & k_{79} & 0 & k_{711} & k_{712} \\ & & & & & & & k_{88} & k_{89} & c_{810} & k_{811} & k_{812} \\ & & & \text{Sym} & & & & & k_{99} & c_{910} & k_{911} & k_{912} \\ & & & & & & & & & k_{1010} & c_{1011} & c_{1012} \\ & & & & & & & & & & k_{1111} & k_{1112} \\ & & & & & & & & & & & k_{1212} \end{bmatrix}$$

Figure 5: Global stiffness matrix of the structure with the added bend-twist coupling terms c_{ij} in red and torsional stiffness in yellow. $k_{1010} = k_{44}$ is the torsional stiffness.

These new terms will induce a twist angle when the structure is loaded by a bending for or a bending moment and therefore a bending motion when the structure is loaded by a torsional moment. ”FE-BTC” designates the structural method with the BTC approach implemented.
This structural approach is also coupled to a Fluid code in a brick named FS6R to analyze FSI on hydrofoils with BTC. FS6R is fully described in [6] and its organizational chart is presented in Fig. 6. After defining the foil geometry, the materials and the configurations to simulate, the fluid flow is solved by the open source tool AVL which performs a VLM in-viscid 3D calculations on the whole surface and provides the hydrodynamic forces. A viscous correction is then realized with XFOIL which performs 2D viscous simulations and the structural analysis is performs by an in-house code standing on beam theory by finite elements.

As outputs of FS6R calculation, we get the efforts applied on the structure and the bending and twist motion characterizing distorted shape.

3 Mechanical tests in air

This chapter describes the tests performed in air on the hydrofoils and the results are compared to the BTC approach described in the previous chapter.

3.1 Description

Mechanical experiments are performed in air, using facilities mounted as a bench test for this purpose at the French Naval Research Academy. The experimental setup is presented in Fig 7, the foil is clamped free on a marble table with clamp seals and a laser is mounted above the structure on a rail that can move in the chord direction.

Three type of loading are performed in these tests:

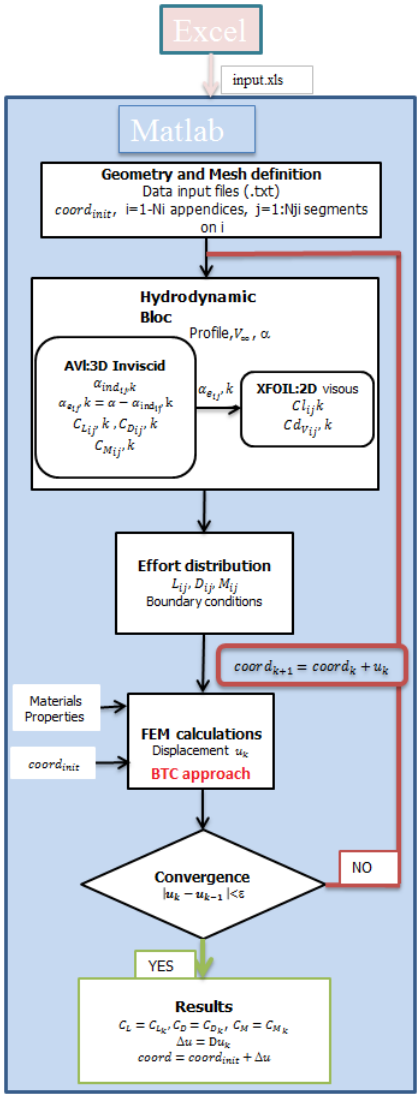

Figure 6: FS6R organizational chart.

Figure 7: Experimental setup of the mechanical tests.

- Torsional loading: A punctual load, off-center as shown in Fig 7 (right-top) is applied on the structure. To only allow twist motion, the foil is placed on a vertical spike blocking the bending

motion. The laser measures the section displacements and the results expected are the torsional modulus and the twist motion.

- Bending loading: A punctual load is applied in the middle section of the tip and the laser measures the displacements. This test will show if the BTC phenomenon appears with the layup investigated. The results expected are the bending stiffness of the foils, the bending motion and a bend twist angle.

- Combined loading: A punctual load, off-center as shown in Fig 7 (right-bottom) is applied on the structure. the bending and twist motion are allowed and the laser measures the section displacements. In this case we expected a bending motion similar as the bending loading case and twist angle equivalent to the sum of the previous two cases.

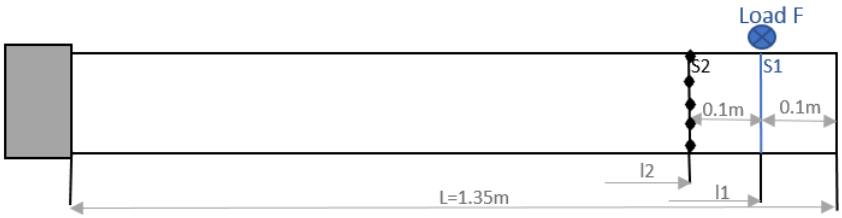

Figure 8: Hydrofoil geometry and measurements positions.

Figure 8 shows the measurements position on the foils. For all the loading type, the load is applied on the section S_1 located at $1.25m$ from the root and the laser measures the vertical displacements Y of the section S_2 distant of $0.1m$ from S_1. 5 points equally located on S_2 are measured and a continuous measurement of the entire section is also recorded.
Four calibrated masses are used for the torsional loading: $M_1 = 2.22kg$, $M_2 = 3.88kg$, $M3 = 5.53kg$ and $M_4 = 7.76kg$, the lever arm is $22.5mm$ from the foil axis. In the bending and combined loading,only M_1 is tested.

3.2 Results

The stiffness modulus experimentally obtained will be presented and the bending and twist motion will be compared to the results from the approach described in the previous chapter. The relation used to calculate these stiffness are given in Eq.5

$$EI = \frac{F \times l_2^2 \times (3l_1 - l_2)}{6Y} \qquad GJ = \frac{M_t \times l_2}{\theta} \tag{5}$$

3.2.1 Torsional loading

Figure 9 shows the twisted section S_2 measured in the loading case M_4. The load is applied on the right side of the section so we observe a well defined rotation of $\theta = 5.43°$ in the clockwise.

The torsional modulus calculated with Eq.5, using the twist angles are presented in Table 2. According to the glass 2 (Table 1), P_1 has the highest modulus. We expected P_2 and P_3 's modulus to be close and P_4 slightly higher than them but the results show $P_4 < P_3 < P_2$.

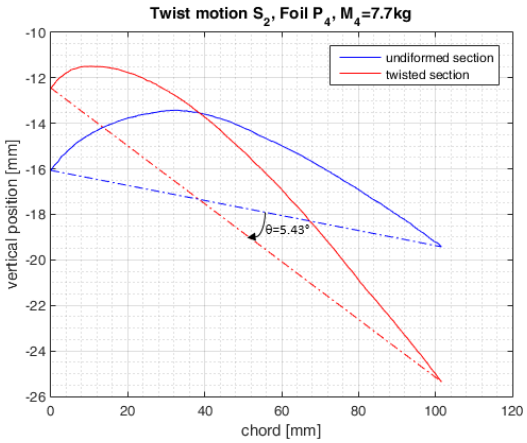

Figure 9: Twisted Section S_2 for P_4

Foil Layup	P_1	P_2	P_3	P_4
$GJ\ [N.m^2]$	290.39	216.3	203.3	186.95

Table 2: Torsional stiffness GJ of the different foils

The experimental twist angles recorded at S_2 for all the layups and the loading masses are compared to the results from our structural approach "FE", in figure 10. The relative discrepancies between the two set of data is also presented.

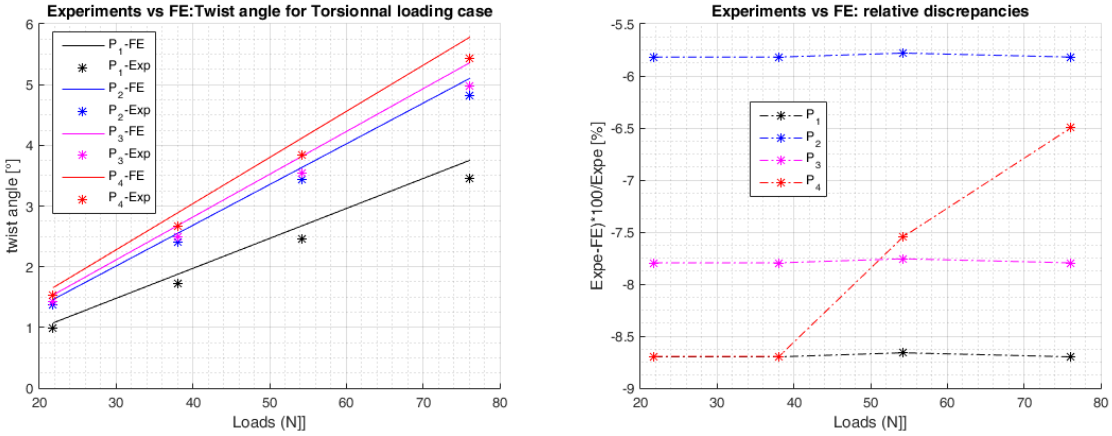

Figure 10: Twist angle for the torsionnal bending measured at section S_2

In agreement with the torsional modulus, for the same applied load, the twist angle is highest for P_4, followed by P_3, P_2 and P_1 is the smallest.
The results computed with our "FE" method are higher than the experimental values. This observation indicates an underestimation of the torsional modulus that may be due to the experimental implementation and the data processing method. Looking at the relative discrepancies, the difference is relatively low and we should expect relative error less than 9% on the twist calculation.

3.2.2 Bending loading

Figure 11 compares the experimental displacement of the foils to the "FE-BTC" calculations, and the bending stiffness calculated by Eq.5 are given in table 3.

According to the ply's properties, P_4 has the highest bending stiffness twice as high as the others, P_1 is higher than P_2 and P_3 in a narrow range. The difference between P_2 and P_3 is likely due to the manufacturing process.
The same observation is repeated with the displacements: the highest stiffness of P_4 leads to the smallest displacement when the smallest stiffness of P_3 leads to the highest displacements. The results of the "FE-BTC" approach are in good agreements with the experiments.

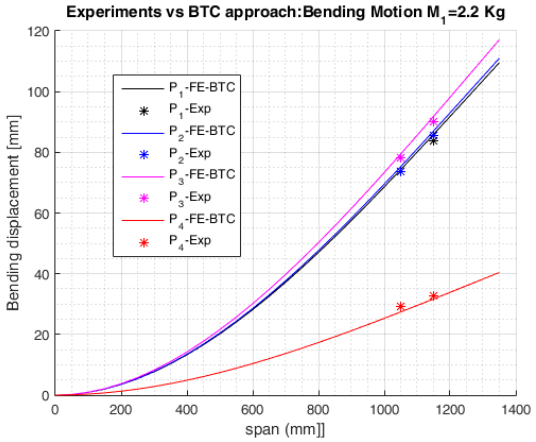

Figure 11: Bending motion of the foils for load M_1

Foil Layup	P_1	P_2	P_3	P_4
$EI\ [N.m^2]$	155.6	153.8	145	420.5

Table 3: Bending stiffness EI of the different foils

To link the bend twist angle to the flow's angle of attack in a hydrodynamic loading, figure 12 shows the sign convention of the angle of attack with the profile orientation. Z clockwise rotation is positive when the counter clockwise is negative.

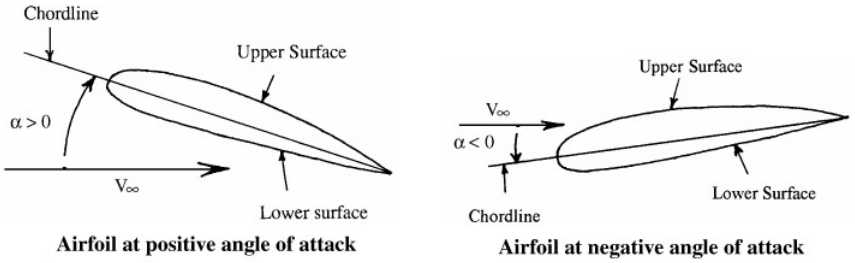

Figure 12: sign convention for the angle of attack on a profile

Figure 13 shows the experimental twist of the section S_2 measured for P_2 and P_3 in the bending loading case. The difference observed on the initial shape of S_2 in the two layups, highlight a difference on their natural bending and therefore the stiffness bending, in agreement with table 3.
According to the sign convention of the angle of attacks, P_2 with $-45°$ in its layup depicts a negative twist when P_3 with $45°$ in its layup experiences a positive twist. The amplitude of P_2 twist ($-1.05°$) is 4% higher than P_3 ($1.01°$).

Figure 14 compares the experimental bend twist angle (measured at S_2 and S_3) for all the layup with the results of the "FE-BTC" approach.

The "FE-BTC" computes a zero twist angle for P_4 and P_4. Theirs layups composition give a bend twist coupling coefficient null, when a small experimental twist of $0.1°$ were recorded for P_1 and P_4. The

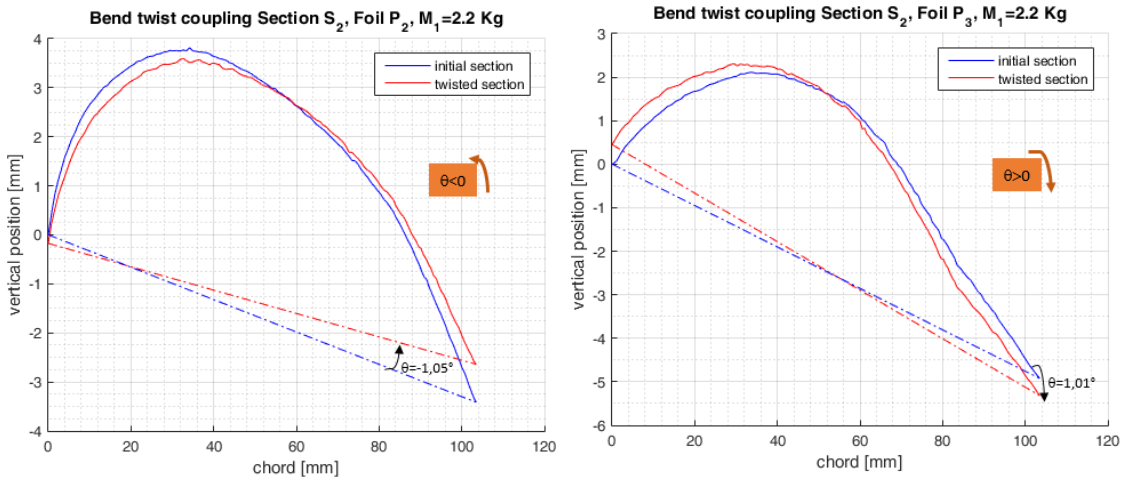

Figure 13: Bend twist angle measured for P_2 and P_3 atS_2, with M_1 load

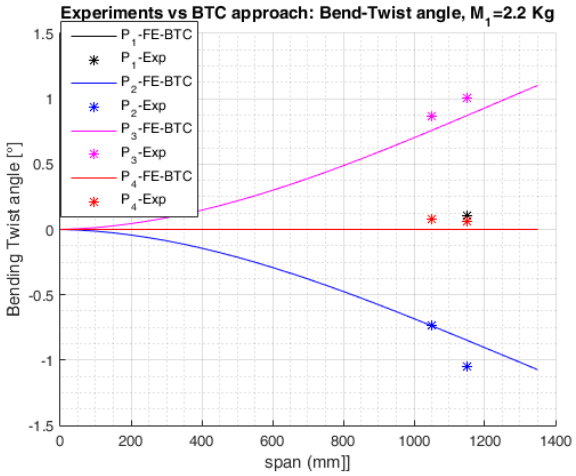

Figure 14: Bend twist angle: Experiments VS "FE-BTC" approach.

trend observe for P_4 and P_3 are the same as the experiments but we observe some discrepancies less than 10%.
The discrepancies observed on the twist angle are most likely due to the experimental implementation. It were found out that the clamp seal were not totally rigid and during the tests the position of the measurement points along the chord may have changed, leading to a direct impact on the twist angle calculation.

As a conclusion of this part, the bend twist coupling phenomenon appears with a good amplitude for P_2 and P_3 layups: P_2 experiences a negative twist when P_3 have a positive twist angle.

3.2.3 Combined loading

The vertical displacement recorded in this loading case is the same as the bending loading. The figure 15 shows the twist of section S_2 for P_2 and P_3 layups. Both layups experience a positive twist corresponding as the sum of bend twist effect and the torsion effect. An accidental modification in the acquisition frequency of the laser is responsible of P_3 un-smooth shape.

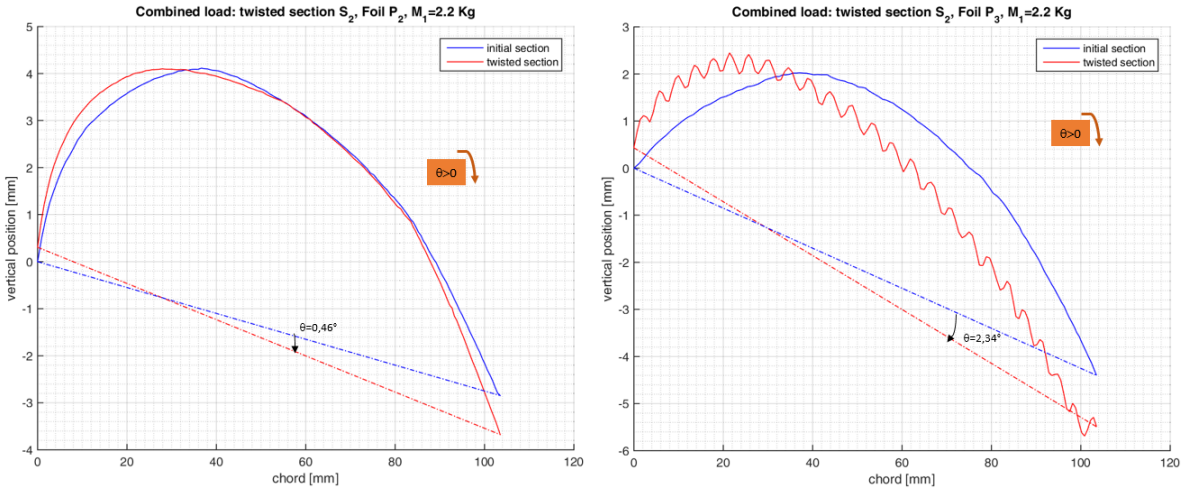

Figure 15: Twisted section S_2 for P_2 and P_3 in combined loading of $M_1 = 2.2kg$.

Table 4 summarizes the experimental twist angle recorded at S_2 for the three loading case with M_1 and the table 5 shows the results from "FE-BTC" approach.

Twist angle [°]	P_1	P_2	P_3	P_4
Torsion	0.99	1.38	1.42	1.5
Bending	0.1	-1.05	1.01	0.06
Combined	No data	0.468	2.34	1.73

Table 4: Experiments

Twist angle [°]	P_1	P_2	P_3	P_4
Torsion	1.07	1.46	1.53	1.65
Bending	0	-0.85	0.87	0
Combined	1.02	0.56	2.36	1.60

Table 5: BTC approach

The twist angle in the combined case appears to be the sum of the bending loading and the torsional loading as expected. "FE-BTC" approach is in good agreement with the experiments and the relative discrepancies are under 15%. We expect lower discrepancies with the hydrodynamic experiments with a clamped system better set (bolts instead of clamp seals).

4 Hydrodynamic experiments with FSI

The mechanical experiments in air shown the appearance of BTC phenomenon for P_2 and P_3 layups. In this chapter hydrodynamic experiments are performed on the hydrofoils to see the impact of the BTC on their hydrodynamic performances. Experimental measurements will also be compared to FS6R results to validate the BTC approach in the case of FSI.

4.1 Description

Hydrodynamic experiments are carried out at IFREMER Lorient in the flume shown in Fig 16. The working section is $2.5m$ in the flow direction and $1.5m$ depth with a maximum velocity of $1m/s$.

The foil is piercing the free surface and is clamped to a 6-DOF balance measuring the efforts and moments (express in the references frame of the foil (X,Y,Z)). In the initial position, the foils are set with an angle of $45°]$ with the free surface. This position helps to remain close to the laser and maximizes the immersed surface with a low confinement effect.
The lateral displacements of the foils are measured at 3 different heights with a laser telemeter through

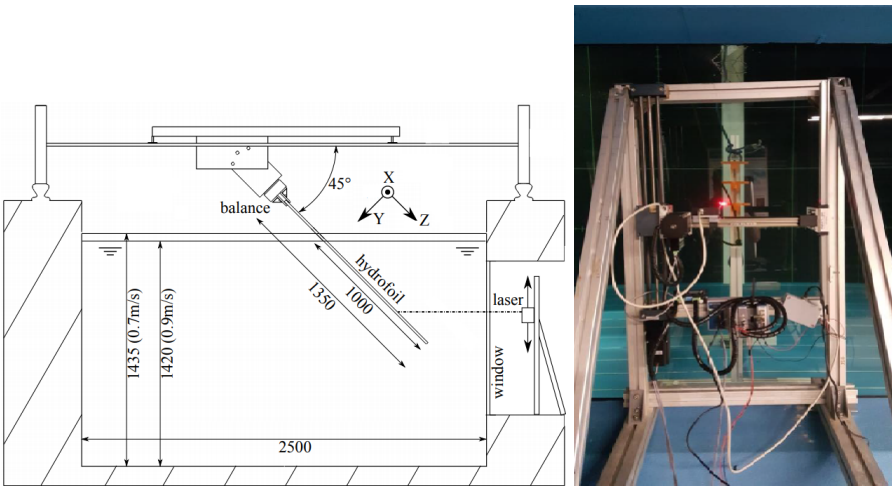

Figure 16: Left: Experimental setup of the hydrodynamic experiments and the calibration set up for the Laser telemeter system. Dimensions are in mm.

the underwater window. A calibration process prior performed to correct the diffraction effect due to the different interfaces that the laser encounters.
The flow is aligned with X-axis. Two speeds $0.7m/s$, $0.9m/s$ and several angles of attack ranging from $[-9°, 0°]$ are investigated. As most of flume, the free surface height varies with the velocity: $1.435m$ for $0.7m/s$ and $1.42m$ for $0.9m/s$.

4.2 Results

The twist angle leading to the modification of the flow's angle of attack impacts the lift, drag forces and therefore the structural displacements. Thus, BTC investigation is performed through the analysis of the hydrodynamic forces and the structural displacements of the hydrofoils.

4.2.1 Impact of BTC on the hydrodynamic performances of the hydrofoils

Figure 17 shows for all the hydrofoils, the lift force in all the configurations investigated. The displacements are also shown for $0.9m/s$ at $-7°$.

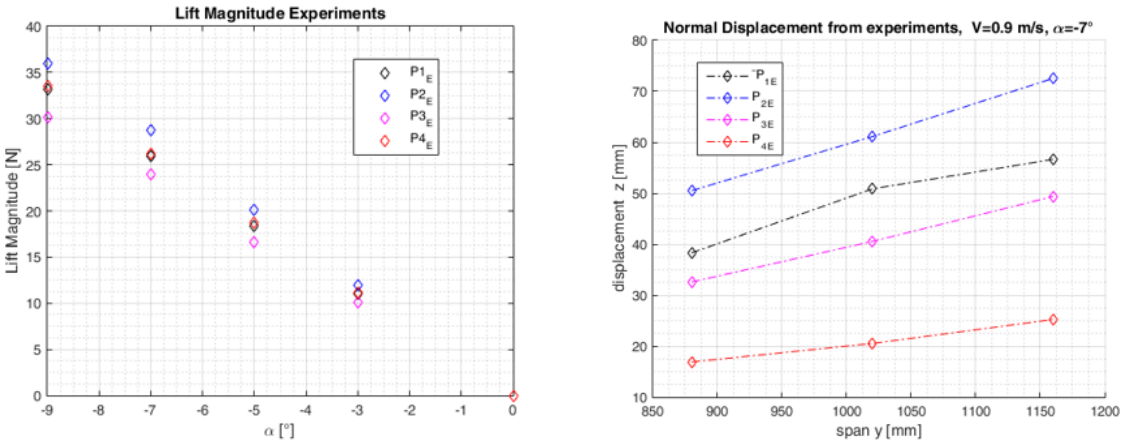

Figure 17: Hydrodynamic forces on the hydrofoils

The lift force clearly exhibits the different behaviors of the layups: P_1 and P_4 overlap as expected from the experiments in air, highlighting no bend twist effect, the results are only linked to the hydrodynamic shape. P_3 is smaller than the P_1, P_4 and P_2 is the highest. This behavior is exactly what we expected according to the results of the experiments performed in air. Because negative incidence is investigated, P_2 with the negative twist is the most loaded when P_3 with the positive twist become the less loaded.

The displacements highlight different behaviors that are linked both to the materials tested (stiffness) and the composite layup (BTC). The carbon foil P_4 is significantly more rigid than the glass fiber foils and it experiences the lowest displacement with $40mm$ at the tip (3% of its span length). We observed at the tip displacements up to $77mm$ (5.8% of span) for P_3 glass fiber foil and only $68mm$ (5.01%) for the P_2 with the same type of laminate (P_2 and P_3 only differs by the plies orientation of $-45°$ for P_2 and $+45°$ for P_3 .$P1$ displacement is higher than $P_3 < P_1 < P_2$) in agreement with BTC effect observed on the lift forces.

4.2.2 Experiments VS FS6R

Figure 18 shows a comparison of FS6R and experimental measurements on the the lift force, in all the configurations investigated and the displacements for $0.9m/s$ at $-7°$. The previous observations on experimental results are perfectly repeated with FS6R simulations and both results overlap very well.

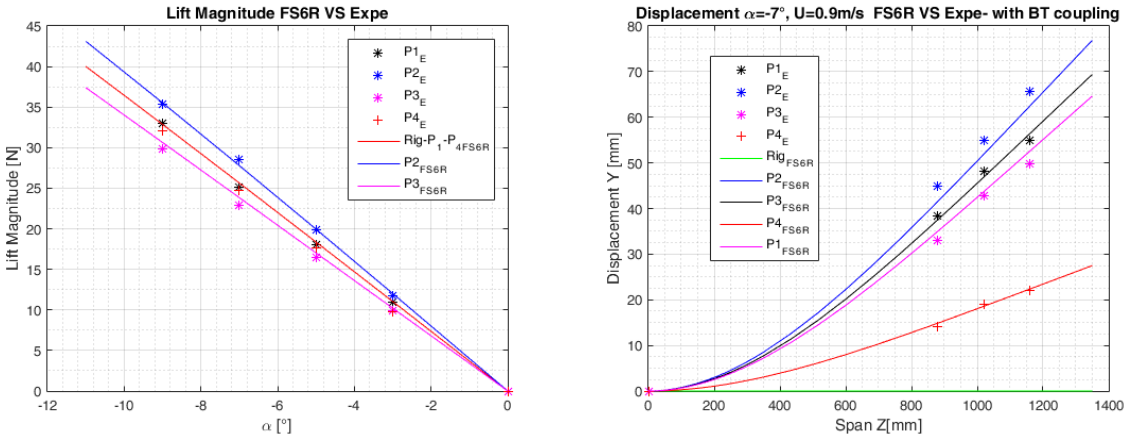

Figure 18: comparison of the experimental displacement of the foils VS FS6R calculations.

The coupling terms c_{ij} added in the stiffness matrix, described in chap 1, differentiates significantly the simulated displacements and forces of P_2 and P_3, and lead to a good fit of the experimental results with overall discrepancies less than 5%.

5 Conclusion

This work presented an experimental and numerical study of the bend twist coupling effect on four composite hydrofoils with the same hydrodynamic shape and different composite layups.
Mechanical experiments performed in air lead to the bending stiffness and torsional modulus of the structures. These tests also show a BTC effect on the layups P_2 and P_3 leading to a positive twist with P_3 and a negative twist with P_2. A comparison of the method implemented to approach BTC effects with air experiments give good results.

Hydrodynamic experiments performed on the hydrofoils in a flume were in good agreement with the test performed in air. No bend twist coupling is observed for $P4$ and $P1$, showing the same lift force. Their displacements were different due to their bending stiffness
That experiments performed with negative incidences clearly highlight the impact of bending-twisting coupling. The foil P_2, with oriented plies at $-45°$ in the laminate, experiences a significantly higher displacement and hydrodynamic loads due to its negative bend twist angle enhancing the angle of attack. P_3, with oriented plies at $45°$, experiences smaller displacements and the smallest hydrodynamic loads due its positive bend twist angle decreasing the angle of attack.
The comparison of experimental results with FS6R computations give very good agreements (discrepancies are less than 10%), showing the ability of the code to compute the bending-twisting coupling.
FS6R has proven to estimates greatly the tendencies of the hydrodynamic loads and the structural motion, which is the first step of the foil design process.

References

[1] R. Balze, N. Bigi, K. Roncin, J. Leroux, A. Nême, V. Keryvin, A. Connan, H. Devaux, and D. Gléhen. Racing. *Innovsail International Conference, Lorient, France*, pages 51–58, 2017.

[2] M. Capellaro. Design challenges for bend twist coupled blades for wind turbines and application to standard blades. In *Proceedings of Sandia Wind Turbine Blade Workshop*, 2012.

[3] O. Gozcu, T. Farsadi, C. Tola, and A. Kayran. Assessment of the effect of hybrid grfp-cfrp usage in wind turbine blades on the reduction of fatigue damage equivalent loads in the wind turbine system. In *Proceedings of the 9th International Workshop on Water Waves and Floating Bodies (10.2514/6.2015-0999)*, 2015.

[4] D. H. Hodges. *Nonlinear Composite Beam Theory, .* 78-1-56347-697-6. American Institute of Aeronautics and Astronautics, 1, 2006.

[5] S. E. Rohde, P. G. Ifju, B. V. Sankar, and D. A. Jenkins. Experimental testing of bend-twist coupled composite shafts. *Experimental Mechanics*, 55(9):1613–1625, 2015.

[6] O. F. V. Temtching, B. AUGIER and J.-A. A. D.R. An experimental and numerical study of fsi applied to sail yacht flexible hydrofoil with large deformations. In *Proceedings of 9th International Symposium on Fluid-Structure Interactions Flow-Sound Interactions Flow-Induced Vibration and Noise (Toronto Canada)*, 2018.